Cold Regions Science and Technology 155 (2018) 1–10

Contents lists available at ScienceDirect

Cold Regions Science and Technology

journal homepage: www.elsevier.com/locate/coldregions

Numerical simulation of heat transfer of the crushed-rock interlayer embankment of Qinghai-Tibet Railway affected by aeolian sand clogging and climate change

Lin Chen[a,c,d], Wenbing Yu[a,b,*], Xin Yi[e], Da Hu[a], Weibo Liu[a]

[a] State Key Laboratory of Frozen Soil Engineering, Northwest Institute of Eco-environment and Resources, CAS, Lanzhou 730000, China
[b] College of Civil Engineering, Chongqing Jiaotong University, Chongqing 400074, China
[c] Cold regions geomorphology and geotechnical laboratory, Department of Geography, University of Montreal, Montreal H2V 2B8, Canada
[d] Centre for Northern Studies, University of Laval, Quebec, Canada
[e] School of architecture and surveying & mapping engineering, Jiangxi University of Science and Technology, China

ARTICLE INFO

Keywords:
Qinghai-Tibet Railway
Climate change
Permafrost degradation
Crushed-rock interlayer
Aeolian sand

ABSTRACT

The crushed-rock interlayer (CRI) has been used to cool the railway embankment subbase and subgrade of the Qinghai-Tibet Railway (QTR) in permafrost regions. However, in addition to the climate change, aeolian sand clogging has been affecting this mitigation techniques aimed to increase heat extraction and reduce subsurface heat penetration by air convection through the voids of the CRI. Its long-term performance is evaluated herein using a numerical modelling. Simulation results demonstrate an unclogged CRI can mitigate permafrost warming for the first 20 years with a simulated increase in average air temperature by 0.052 °C a^{-1}. But after sand clogging, including both filling of voids in the CRI and covering of embankment slopes, its cooling performance is weakened. In such conditions, permafrost table is increasing and the permafrost is warming up under different mean annual air temperature (MAAT) of −4.5, −5.5, and −6.5 °C. The water content of the aeolian sand can also affect the cooling effectiveness of CRI. A 1 m-thick dry sand cover can induce an increase in ground temperature. But wet sand layer can mitigate and delay the effect of climate change on the permafrost degradation. The sand-control measures and additional engineering techniques should be adopted to prevent the long-term thermal stability of the QTR in sandy permafrost zone of Qinghai-Tibet Plateau.

1. Introduction

The crushed-rock interlayer embankment (CRIE) has an excellent cooling performance and has been widely used to insure the thermal stability of railway embankment in permafrost regions of Qinghai-Tibet Plateau (QTP) (Cheng, 2005; Doré et al., 2016; Goering and Kumar, 1996; Harris and Pedersen, 1998; Lai et al., 2014; Ma et al., 2009; Wu et al., 2002). Based on its cooling characteristic, there are two types of CRIE: 1) open CRIE and 2) closed CRIE, which has been experimented at the QTP (Dong et al., 2014; Hou et al., 2015; Liu et al., 2017; Mu et al., 2012; Sun et al., 2011; Wu et al., 2008; Zhang et al., 2016), North-Eastern China, Alaska (Darrow and Jensen, 2016; Xu and Goering, 2008) and north Canada (Malenfant-Lepage et al., 2012). In winter when the wind blowing is strong in the QTP, intensive convection of air through the voids of an open CRIE increases considerably the effective heat extraction in the permafrost subgrade (Goering, 2003; Goering and Kumar, 1996). While, in the case of a closed CRIE, a thin geomembrane and soil layer covered on the embankment slopes not only prevent warm wind incursion into the CRI during the summer, but also impedes the water infiltration from the surface. Therefore, the cooling effect of closed CRIE only depends on natural convection occurring in the coarse materials which is driven by gradient in air density due to variations in temperature in this interlayer (Malenfant-Lepage et al., 2010; Yu et al., 2004; Yu et al., 2016). However, if the temperature boundary conditions of the CRI surface change over time, the heat transfer processes and the cooling effect of CRIEs can be adversely affected. For instance, aeolian sand clogging of voids in open CRIE can impede the air convection under strong wind blowing in winter. Also, the upper layer of open CRIE slope may be obstructed by sand and gravel from winter maintenance operations (Malenfant-Lepage et al., 2012). While a thick snow or aeolian sand cover on embankment slopes can insulate both open and closed CRIEs.

Human activities and increasing air temperature have caused significant grassland degradation and desertification on the QTP (Cheng

* Corresponding author at: State Key Laboratory of Frozen Soil Engineering, Northwest Institute of Eco-environment and Resources, CAS, Lanzhou 730000, China.
E-mail address: 99155644@qq.com (W. Yu).

https://doi.org/10.1016/j.coldregions.2018.07.009
Received 16 January 2018; Received in revised form 25 May 2018; Accepted 19 July 2018
Available online 20 July 2018
0165-232X/ © 2018 Elsevier B.V. All rights reserved.

Fig. 1. Photograph of aeolian sand clogging and accumulation of a CRIE along the QTP.

and Wu, 2007; Harden et al., 2012; Sivakumar, 2007; Wu et al., 2017). Following the impacts, the performance of CRIEs has been affected by aeolian sand transportation and deposition since 2006 and this process is still rapidly spreading along the QTR (Xie et al., 2017; Zhang et al., 2010). In 2008, 25% of the total length of the GerLha section of QTR, a cumulated stretch of about 270 km long, is affected by this process (Fig. 1). The impacts of aeolian sand deposition along railway embankment on the cooling effectiveness of CRIE can be classified into two categories: 1) the aeolian sand clogging in open CRIE reduces the permeability of CRI to air and the heat extraction in the permafrost subgrade, and 2) the aeolian sand accumulation on open and closed CRIE slopes induces thermal insulation and modifies the absorption of solar radiation. Moreover, the air temperature in the QTP is projected to increase about 2.2–2.6 °C by 2050 (Qin et al., 2002; Solomon et al., 2007).

Research found aeolian sand clogging can weaken the cooling effectiveness of CRIE (Chen et al., 2015; Chen et al., 2017; Yu et al., 2016). However, the complex interaction between CRIE, aeolian sand clogging and deposition, and underlying permafrost remains poorly understood and quantified. The long-term thermal performance of CRIE under the combined influence of aeolian sand clogging and climate change has not yet been studied. The cooling effectiveness of CRIE affected by aeolian sand clogging is assessed herein using a numerical modelling approach supported by field measurements. A two-dimensional finite-element model was used to simulate the impacts of climate change and aeolian sand clogging of CRIE on its cooling performance under different mean annual air temperature (MAAT) of −4.5, −5.5, and −6.5 °C. In addition, three different permafrost types and two water contents of the aeolian sand are considered.

2. Model description

A two-dimensional finite-element model similar to the one developed by Lai et al. (2003); and (2006) was used to model the heat transfer in CRIE. The control-volume integration method is adopted to discretize the time and space of governing equations and the maximum normalized changes of all variables are 10^{-6} (Tao, 2001; Zhang et al., 2015). The numerical model adopted in this study has been calibrated by the field measurements (Yu et al., 2016). This numerical modelling is supported by field investigation conducted at Honglianghe in QTP since 2012 to describe the aeolian sand clogging and accumulation along the QTR and characterize the thermal properties of materials in CRIE subbase and subgrade, and the boundary conditions at the surface of CRIE.

2.1. Conceptual model of the CRIE

The conceptual model of the CRIE is shown in Fig. 2. Because of the symmetry of physical domain and heat transfer in the closed CRIE, half of the closed CRIE relative to the embankment centerline was simulated. Results from excavation of berms revealed the presence of completely blocked crushed-rock interlayer (CRI) at the embankment slope. The aeolian sand clogging and deposition can decrease the effective porosity of the CRI and modify the surface temperature. According to the investigation along the QTR, a large volume of aeolian sand can fill up the voids in the CRI of open CRIE, especially at both toe and slope of open CRIE (See Fig. 1). Therefore, in our simulated model, we assumed that the aeolian sand fill up the voids in the CRI of open CRIE berms. Moreover, the characteristic length of aeolian sand deposition at the embankment toe is 4 m with a maximum thickness from 0.2 to 1.0 m (Fig. 3), based on the field investigation. The characteristic length also agrees with other research done in the Qinghai-Tibet Plateau (Xie et al., 2015; Zhang et al., 2010). Such changes in surface conditions of CRIE are considered as moderate to severe degree of aeolian sand deposition (Zhang et al., 2010).

2.2. Thermal properties of materials in CRIE

The thermal and physical parameters were conducted in the lab and details can be found in the reference (Chen et al., 2014). The thermal properties of embankment materials can be found in the reference (Xu et al., 2001). The effective thermal conductivity of sand-filled CRI was calculated by geometric mean method (Farouki, 1981) and the effective heat capacity was assessed by the arithmetic mean method (Fortier et al., 2011). The thermal properties of the different layers of the model illustrated in Fig. 2 are given in Tables 1 and 2. The intrinsic permeability and inertial resistance factor were calculated based on the average diameter and porosity of crushed rock (Chen et al., 2017; Zhang et al., 2006a). Also, the intrinsic permeability of aeolian-sand-filled rock layer is $0.84 \times 10^{-9}\,m^{-2}$ and its porosity is 0.16. The density and dynamic viscosity of air at an average elevation of 4600 m for the QTP is $0.641\,kg\,m^{-3}$, $1.75 \times 10^{-5}\,kg\,m^{-1}\,s^{-1}$, respectively. Its specific heat capacity and thermal conductivity are $1.004 \times 10^{3}\,J\,kg^{-1}\,K^{-1}$ and $0.02\,W\,m^{-1}\,K^{-1}$ respectively (Zhang et al., 2006a).

2.3. Boundary conditions of the conceptual model of CRIE

To simplify the boundary conditions and represent the complex heat transfer at the surface, the annual surface temperature is approximated by a sinusoidal function (Carson, 1963). According to the measured air temperature in QTP and the boundary layer theory (Carson, 1963; Zhu, 1988), the top surface temperatures T in this study are defined as a sinusoidal function with a seasonal temperature amplitude of A and a temperature increment B (See Eq. 1). The temperature increment is adopted to represent solar radiation absorbed by the bare dark surface of embankment material due to change in albedo (Table 3). From 0 to 50 years, the warming rate is $0.052\,°C\,a^{-1}$ and represents the average rate of air temperature increase from the QTP climate projections (Qin et al., 2002). Values of temperature correction factor and seasonal temperature amplitude in air temperature are given in Table 3 for different surface conditions according to the field observations.

$$T = T_a + B + \alpha \cdot t + A\sin\left(\frac{2\pi \cdot t}{8760} + \varphi\right) \quad (1)$$

where T_a is the mean annual air temperature (°C), B is the temperature increment (°C) based on the boundary layer theory (Zhu, 1988), $\alpha$is the rate of climate change ($°C\,a^{-1}$), A is the seasonal temperature amplitude (°C), t is the time (hour), and $\varphi = \pi/2$ is the phase shift (radian).

Based on and on the “power law of wind profile” and on the observed data in the QTP (Zhang et al., 2006b; Zhao et al., 1991), the variations in wind velocity with the height relative to the ground surface at input boundary is given by:

$$v_{10} = 4.0 + 1.21\sin\left(\frac{2\pi}{8760}t + \varphi\right) \quad (2)$$

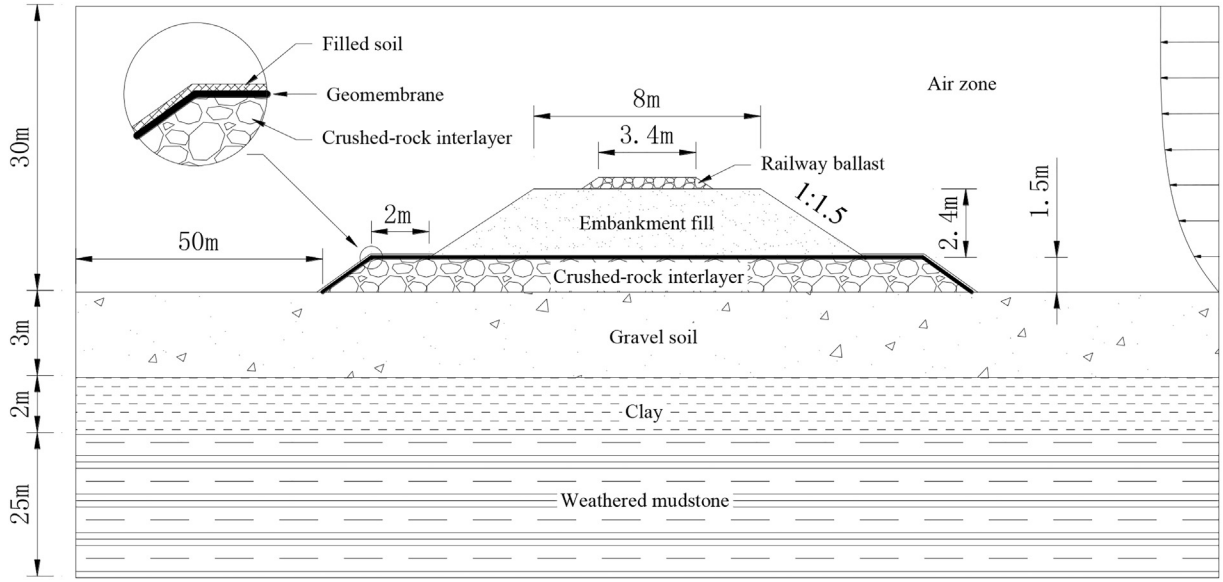

Fig. 2. Geometric model and strata used for the numerical modelling. A thin geomembrane and soil layer are covered on the slope of closed CRIE, while open CRIE is uncovered and without geomembrane.

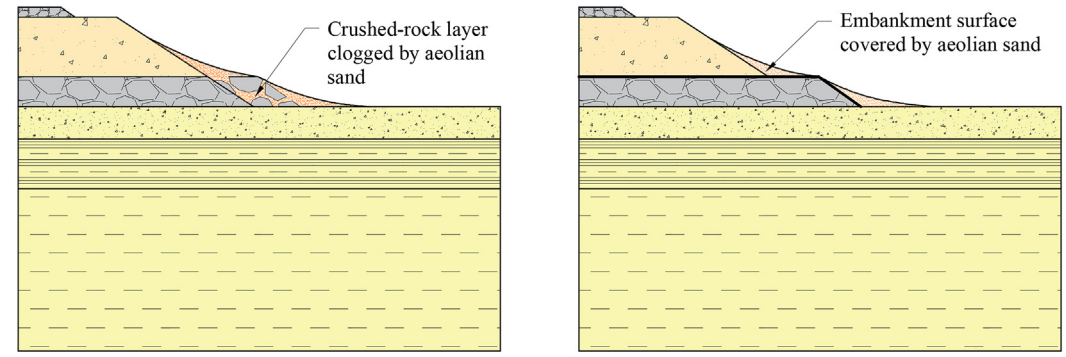

(a) Open CRIE clogged and covered by aeolian sand (b) Closed CRIE covered by aeolian sand

Fig. 3. Cross sections of the railway embankment. The aeolian sand clogging in open CRIE reduces the permeability of CRI to air, and the aeolian sand accumulation on open and closed CRIE slopes changes the surface boundary condition.

$$v_z = v_{10}\left(\frac{z}{10}\right)^{0.16} \quad (3)$$

where v_{10} is the wind velocity at a height of 10 m (m s^{-1}), v_z is the wind velocity at a given height z (m s^{-1}), z is the height relative to the ground surface (m), t is the time (hour), and $\varphi = 4\,\pi/3$ is the phase shift (radian).

As there is no horizontal heat transfer in a semi-infinite body, an adiabatic boundary condition is applied on both sides of the conceptual model of CRIE (Fig. 2). A geothermal heat flux of 0.06 W m^{-2} is assigned across the bottom of the domain (Yu et al., 2014).

2.4. Modelling sequence

The numerical modelling of the thermal regime of open and closed CRIEs affected by both aeolian sand clogging and accumulation, and climate change was performed over a simulation period of 50 years after the QTR completion. Aeolian sand clogging and accumulation in the field is the most likely to occur over the first year following completion of the railway embankment, in the numerical modelling carried out as an abrupt event during 10th year of the simulation period. At that moment, the CRIE was considered entirely clogged and covered by

Table 1
Thermal properties of the model layers.

	λ_f W m^{-1} K^{-1}	C_f J m^{-3} K^{-1}	λ_u W m^{-1} K^{-1}	C_u J m^{-3} K^{-1}	L J m^{-3}
Ballast	0.346	1.001×10^6	0.346	1.001×10^6	0.0
Embankment fill	2.053	1.625×10^6	1.794	1.982×10^6	2.040×10^7
Sand-free crushed rock	0.442	1.016×10^6	0.442	1.016×10^6	0.0
Sand-filled crushed rock	1.187	1.465×10^6	1.187	1.465×10^6	0.0
Gravel soil	2.610	1.863×10^6	1.910	2.401×10^6	2.318×10^7
Clay	2.120	2.542×10^6	1.420	3.345×10^6	6.515×10^7
Weathered mudstone	1.824	2.122×10^6	1.474	2.413×10^6	3.811×10^7
Dry aeolian sand	0.258	1.610×10^6	0.258	1.610×10^6	0.0
Wet aeolian sand	1.380	1.648×10^6	1.140	2.064×10^6	3.213×10^7

Table 2
Physical properties of different frozen ground conditions.

	ρ kg m^{-3}	W %	λ_f W m^{-1} K^{-1}	C_f J m^{-3} K^{-1}	λ_u W m^{-1} K^{-1}	C_u J m^{-3} K^{-1}	L J m^{-3}
Ice-poor frozen ground	1660	20	1.382	2.207×10^6	1.243	2.677×10^6	6.030×10^7
Icy soil	1540	25	1.580	2.229×10^6	1.127	2.822×10^6	7.015×10^7
Ice-rich frozen ground	1280	35	1.673	2.230×10^6	1.092	2.989×10^6	1.228×10^8

Table 3
Ground surface boundaries of the numerical model.

	Natural ground surface	Aeolian sand surface	Rock layer surface	Gravel surface
Amplitude A (°C)	12.0	14.2	15.2	13.5
Temperature increment B (°C)	4.9	4.4	5.5	4.8

aeolian sand. And two maximum thicknesses of aeolian sand accumulation of 0.2 and 1 m at the CRIE toe were simulated as moderate and severe degrees of aeolian sand deposition, respectively. Also, the mean annual ground temperature (MAGT) and permafrost table beneath the CRIE reach to a stable situation after experiencing a quick and significant decrease at the 10th year after embankment construction (Lai et al., 2003; Zhang, 2007). The thermal regimes of CRIE subbase and subgrade reach a quasi-dynamic equilibrium, and therefore the impact of railway embankment construction can be considered completely dissipated. Finally, the model simulation is run in two phases. The first phase generates a quasi-dynamic equilibrium for the active zone overlain permafrost layer with seasonally varying surface temperature. During the second phase, the embankment zone is activated at the beginning of the 50-year period and the aeolian sand layer is activated at the 10th year. For the results presented below, time is accounted at the starting of phase two. From year 0 to 50, a warming rate of 0.052 °C a^{-1} is used, which is the maximum projected change in air temperature for the QTP (Qin et al., 2002).

3. Results and analysis

3.1. Thermal impacts on the cooling effectiveness of the open CRIE

To assess the impacts of climate conditions on permafrost change underneath an open CRIE clogged and covered by aeolian sand, three numerical simulations under different MAAT of −4.5, −5.5 and −6.5 °C were carried out. Moreover, three different permafrost conditions underneath the open CRIE were considered: ice-poor frozen ground, icy soil, and ice-rich frozen ground in the clay layer of the subgrade (Fig. 2) with respective volumetric ice contents 20%, 25%, and 35% (Xu et al., 2001).

3.1.1. Thermal regime of the open CRIE

The thermal regimes of an open CRIE under a MAAT of −4.5 °C and an air temperature increase rate of 0.052 °C a^{-1} on October 15th of the 30th year after the QTR completion are given in Fig. 4 for three different conditions: 1) a standard railway embankment without a CRI, 2) an open CRIE free of sand, and 3) an open CRIE clogged and covered by aeolian sand.

The temperature distributions of embankment after 30 years of construction were chosen and compared to show the short-term impact of aeolian sand clogging on thermal stability of the railway embankment. This moment of the year in mid-October was chosen because the thawing front has reached its largest depth at that moment and the 0 °C isotherm locates the permafrost table. For the first condition, the CRI was replaced by embankment fill material. The permafrost table underneath the centerline is at the depth of 1.5 m beneath the interface between the embankment and the natural ground. While in the case of the open CRIE free of sand, the permafrost table has moved upward above the natural ground in the CRIE subbase. Moreover, a zone of cold permafrost at a ground temperature of about −2 °C is present directly underneath the railway embankment while the permafrost temperature away from the railway embankment is slightly above −1 °C. As a proof of its cooling effectiveness, the open CRIE has induced permafrost aggradation and restricted the extent of active-layer thickness. This mitigation method are able to counteract the impacts of global climate warming on permafrost warming and thawing some extent. However, due to aeolian sand clogging and accumulation, permafrost table has decreased by 0.5 m underneath the railway embankment centerline. Even if the permafrost table is not anymore in the CRIE subbase but in the subgrade, the permafrost table is still 3.5 m shallower than the one under the natural ground surface away from the railway embankment. However, the ground temperatures at a depth between 5 and 10 m directly underneath the railway embankment is about 1.2 °C warmer for the case with aoelian sand clogging and accumulation than the one without aeolian sand clogging and accumulation. The aeolian sand clogging and accumulation largely reduce the cooling effectiveness of open CRIE and induce subgrade warming.

3.1.2. Variations in permafrost table and ground temperature

The variations in permafrost table under the railway embankment centerline over the simulation period of 50 years for the three initial MAATs of −4.5, −5.5 and −6.5 °C are shown in Fig. 5a. Before the QTR construction, the respective simulated permafrost table were 3.0, 1.8 and 1.3 m for the three constant MAATs. Only one year after the construction of an open CRIE, the permafrost table has moved upward of 3.2, 2.4 and 2.1 m in the CRIE subbase above the natural ground, respectively. Following the next nine years before the aeolian sand clogging and accumulation, the permafrost table has continued to move upward at a rate of only a few centimeters per year. Without aeolian sand clogging and accumulation and with a warming rate of 0.052 °C a^{-1}, the permafrost table remains stable from the 15th to 20th year of the simulation period since the QTR completion. Therefore, in such conditions, the cooling effect of an open CRIE can effectively counteract the impacts of increase in air temperature due to climate change. After 20 years of QTR operation, the permafrost table is progressively deepening and permafrost is warming, but the embankment subgrade temperature is still below 0 °C.

In the cases of aeolian sand clogging and accumulation, which their impacts are fully effective ten years after the QTR completion, the permafrost table has suddenly increased by 0.5, 0.7 and 0.7 m, respectively, for the three initial MAATs of −4.5, −5.5 and −6.5 °C. At the 50th year of the QTR operation, the permafrost table has reached depths of 2.7, 0.5 and 0.2 m below the ground surface respectively. There is still no permafrost degradation compared to the initial permafrost distribution. However, the warm permafrost under a MAAT of −4.5 °C is more vulnerable to the impacts of aeolian sand clogging and accumulation. After 50 years of increase in air temperature due to climate change, the MAAT is now −1.9 °C and the permafrost table at a depth of 2.7 m is now close to the original permafrost table under natural condition before the QTR completion and warming period. Over the last ten years from the 40th to 50th year of the simulation period, a thawing rate of 0.1 m/year is simulated under such conditions. Only few more years are needed for the thawing front to reach the initial

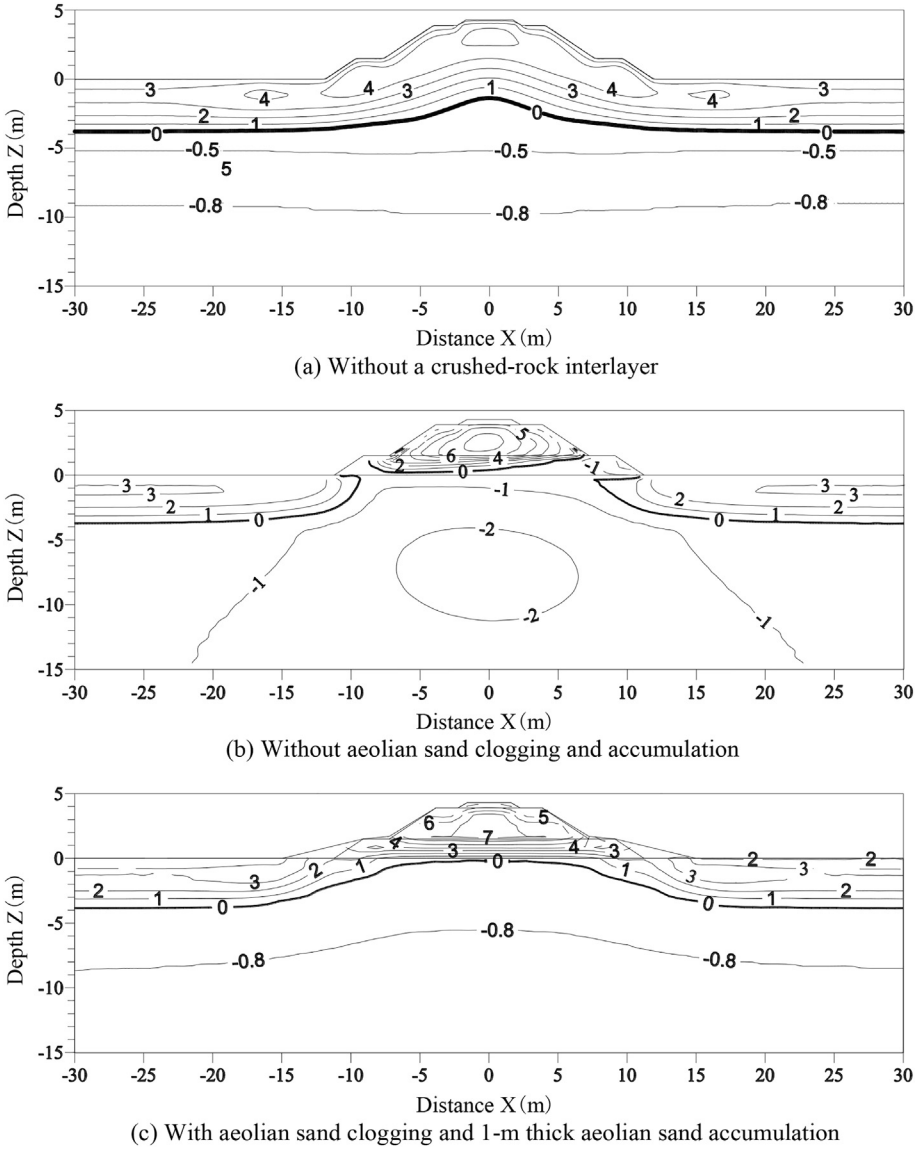
Depth Z (m)
Distance X (m)
(a) Without a crushed-rock interlayer
(b) Without aeolian sand clogging and accumulation
(c) With aeolian sand clogging and 1-m thick aeolian sand accumulation

Fig. 4. Temperature distributions (°C) of the open CRIE on October 15th of the 30th year of climate warming from an initial MAAT of −4.5 °C.

permafrost table and begin the permafrost degradation. For the the initial MAAT of −5.5 °C and −6.5 °C, the original permafrost at depth is now affected over the next decades.

The MAGT variations at a depth of 15 m beneath the ground surface underneath the railway embankment centerline are shown in Fig. 5b. Before the QTR construction, the respective simulated MAGT are −1 °C, −1.4 °C and −2.3 °C for the three MAAT conditions of −4.5 °C, −5.5 °C, and 6.5 °C. For the three MAAT conditions, even under an increase of air temperature at the rate of 0.052 °C a^{-1}, the MAGTs have decreased in excess of 1 °C from the QTR completion to the 20th year of

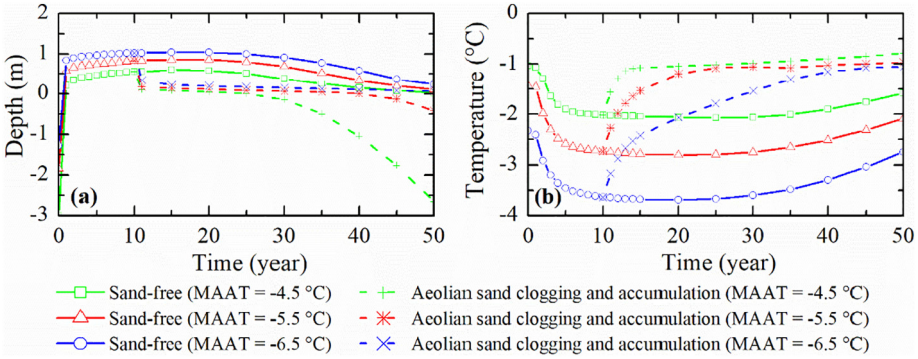
Depth (m)
Time (year)
(a)
Temperature (°C)
(b)
Sand-free (MAAT = -4.5 °C)
Sand-free (MAAT = -5.5 °C)
Sand-free (MAAT = -6.5 °C)
Aeolian sand clogging and accumulation (MAAT = -4.5 °C)
Aeolian sand clogging and accumulation (MAAT = -5.5 °C)
Aeolian sand clogging and accumulation (MAAT = -6.5 °C)

Fig. 5. (a) Variations in permafrost table underneath the railway embankment centerline for an open CRIE. (b) Changes in MAGT at a depth of 15 m beneath the natural ground surface underneath the centerline of open CRIE.

the simulation period for an open CRIE free of sand. From the 20th to 25th year, the MAGTs have remained constant. They have then increased until the end of the simulation period at average rates of ground temperature are 0.011, 0.016, and 0.022 °C a^{-1} for the MAATs of −4.5, −5.5, and −6.5 °C, respectively. However, when the aeolian sand clogging and accumulation become fully effective ten years after the QTR completion, the increase in MAGTs is sharp over the next ten years. The increasing magnitudes of MAGT from 10th to 50th year of the simulation period are 1.2, 1.5, and 2.6 °C for the MAATs of −4.5, −5.5, and −6.5 °C, respectively. At the end of the simulation period, the MAGTs slowly rise to −0.8 °C, −1 °C, and −1.1 °C, respectively. These isothermal conditions are due to the latent heat effect. The more heat propagated downward at depth is needed to induce the phase change and thaw the frozen ground.

Again, the cooling effectiveness of open sand-free CRIE is shown in Fig. 5b even under a context of increase in air temperature due to climate change. This mitigation method can counteract the impacts of air temperature increase due to climate change on permafrost underneath an open CRIE. However, this cooling effectiveness is largely weakened by the aeolian sand clogging of the CRI and accumulation on the railway embankment slopes. Moreover, warm permafrost under a higher MAAT is more vulnerable to the impacts of air temperature increase due to climate change and aeolian sand clogging and accumulation.

3.1.3. Impacts of frozen ground conditions

The thermal responses of different frozen ground conditions (ice-poor frozen ground, icy soil, and ice-rich frozen ground in the clay layer of the conceptual model in Fig. 2) underneath an open CRIE over the simulation period are given in Fig. 6. Both open CRIEs free of sand and clogged and covered by aeolian sand are considered. The climate conditions are a MAAT of −4.5 °C and a warming rate of 0.052 °C a^{-1}. The simulated thickness of dry sand layer located at the railway embankment toe is 1 m. The aeolian sand clogging and accumulation are fully effective the 10th year of the simulation period.

For all frozen ground conditions, by comparing the permafrost tables underneath the railway embankment centerline and toe, the cooling effect of open CRIE is more pronounced at the centerline (Fig 6a, c, and e). The permafrost table underneath the railway embankment centerline has moved upward as much as 3.2 m only one year after the QTR completion, from a depth of 3 m below the original ground surface to 0.2 m in the CRIE subbase, in comparison to only 0.7 m underneath the railway embankment toe, from a depth of 3.2 m to 2.5 m. Over the next nine years, even if the MAAT is increasing, the permafrost table is still moving upward at the embankment centerline and toe while, under the natural ground conditions away from the railway embankment, the permafrost table is increasing right at the beginning of the simulation period. After the 10th year of the simulation period, the permafrost table is increasing for all frozen ground conditions. However, after the aeolian sand clogging and accumulation occurring the 10th year, the cooling effectiveness of open CRIE is weakened and the rate of deepening of permafrost table is quickly increasing over time in comparison to the case where the open CRIE is free of sand. The deepening of permafrost table is more pronounced underneath the railway embankment centerline than the railway embankment toe. Therefore, the aeolian sand clogging has a more pronounced effect on the cooling effectiveness of open CRIE than the aeolian sand accumulation at the railway embankment toe. The deepening of permafrost table over time due to air temperature increase is less pronounced in the cases where the frozen clay layer is ice-rich (Fig. 6e vs Fig. 6a and c). In comparison to the ice-poor and icy frozen ground conditions, the permafrost thawing is delayed in the ice-rich frozen ground because of latent heat of melting ground ice where more heat is needed to induce phase change and fully melt the ground ice.

In Fig. 6b, d, and f, the variations in MAGT at a depth of 15 m beneath natural ground surface over the simulation period are given

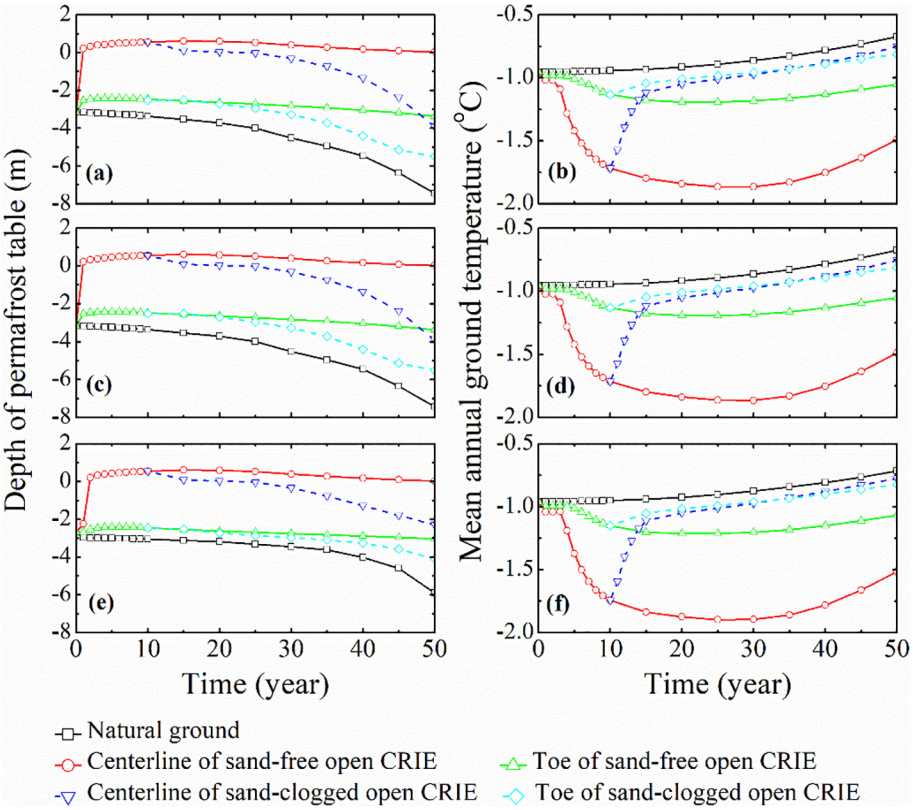

Fig. 6. Variations of permafrost table and MAGT at a depth of 15 m beneath the natural ground surface over a period of 50 years from an initial MAAT of −4.5 °C for ice-poor frozen ground in (a) and (b), icy soil in (c) and (d), and ice-rich frozen ground in (e) and (f).

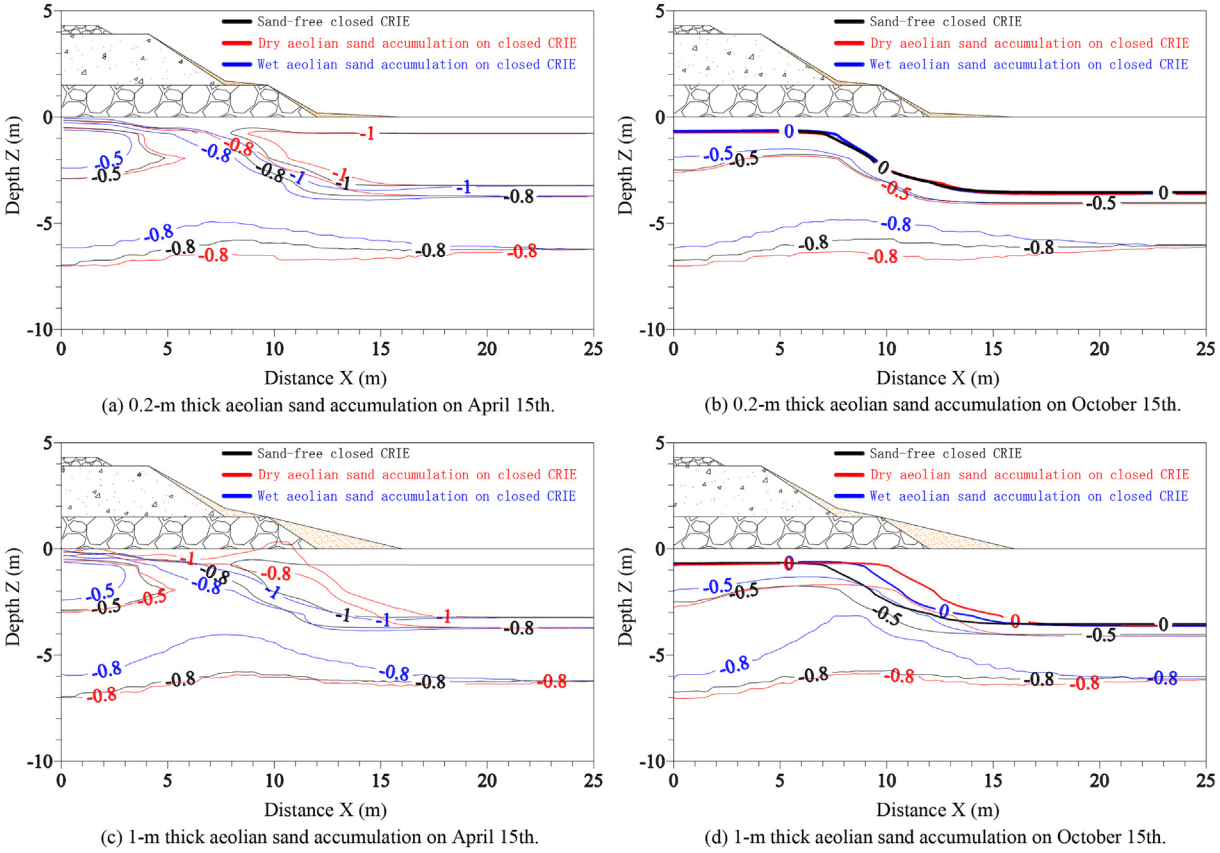
Sand-free closed CRIE
Dry aeolian sand accumulation on closed CRIE
Wet aeolian sand accumulation on closed CRIE
Depth Z (m)
Distance X (m)
(a) 0.2-m thick aeolian sand accumulation on April 15th.
(b) 0.2-m thick aeolian sand accumulation on October 15th.
(c) 1-m thick aeolian sand accumulation on April 15th.
(d) 1-m thick aeolian sand accumulation on October 15th.

Fig. 7. Temperature distributions (°C) of a closed CRIE on April 15th (a and c) and October 15th (b and d) of the 30th year of climate warming from an initial MAAT of −4.5 °C for railway embankment slopes covered by 0.2-m thick aeolian sand layer in (a) and (b), and 1-m thick aeolian sand layer in (c) and (d).

under natural ground conditions and underneath the railway embankment centerline and toe. As previously mentioned, the cooling effectiveness of open CRIE is weakened after the aeolian sand clogging and accumulation and the MAGTs underneath the railway embankment centerline and toe are increasing quickly in such conditions after the 10th year of the simulation period. These MAGTs beneath embankment centerline and toe are closing to the one under natural ground conditions for a difference in MAGTs of < 0.5 °C only 5 years after the aeolian sand clogging and accumulation. By comparing the Fig. 6b, d, and f, the different frozen ground conditions do not noticeably change the variations in MAGT over the simulation period.

3.2. Thermal impacts on the cooling effectiveness of closed CRIE

The impacts of air temperature increase at the rate of 0.052 °C a^{-1} from an initial MAAT of −4.5 °C and aeolian sand accumulation on the cooling performance of a closed CRIE are shown in Fig. 7. Two thicknesses of aeolian sand accumulation of 0.2 and 1.0 m were simulated (thin vs. thick aeolian sand layer). Moreover, two different water contents in the aeolian sand accumulation were considered: 1) 0% and 2) 3% for dry and wet sand conditions respectively. The thermal regimes in the railway subbase of a closed CRIE are given in Fig. 7 for two dates on April 15th and October 15th of the 30th year of the simulation period. As previously mentioned, this moment of the year in mid-October was chosen to locate the permafrost table. But the moment of the year in mid-April is characteristic of the coldest conditions of underlying permafrost.

Using the thermal regime on April 15th underneath a closed CRIE free of sand as a reference, the permafrost temperature underneath the railway embankment in such conditions is colder than the one with a thin dry aeolian sand cover but warmer than the one with a thin wet aeolian sand cover (Fig. 7a). In contrast, the permafrost temperature underneath a closed CRIE free of sand is almost similar to the one for a closed CRIE covered by a thick dry aeolian sand cover but much warmer than the one for a closed CRIE covered by a thick wet aeolian sand cover (Fig. 7c). For instance, the −0.8 °C isotherm at a depth of 6 m underneath the railway embankment centerline of a closed CRIE covered by a thin wet aeolian sand cover is 1 m shallower than the ones of closed CRIEs free of sand and covered by a thin dry aeolian sand cover. Similar conclusions can be drawn underneath the railway embankment toe.

Additionally, similar conclusions can be drawn for the thermal regimes of subgrade on October 15th of the 30th year of simulation period. Using the thermal regime of subgrade underneath a closed CRIE free of sand as a reference, the permafrost table underneath the railway embankment centerline and toes is similar to the one of a closed CRIE covered by thin dry aeolian sand cover (Fig. 7b). The permafrost table underneath a closed CRIE covered by thin wet aeolian sand cover is shallower by a few decimeters than the one underneath a closed CRIE free of sand (Fig. 7b). However, for a thick aeolian sand cover, while the permafrost table is at the same depth for all the cases underneath the railway embankment centerline, this is not the case at the railway embankment toes (Fig. 7d). The permafrost table is much shallower from 1 to 2 m underneath for a thick dry aeolian sand layer at the toes than a thick wet aeolian sand layer or a sand-free closed CRIE. But, the permafrost at depth underneath the toes is warmer under a thick dry aeolian sand layer than a thick wet aeolian sand layer. For instance, underneath the toe at a distance of 12 m, the −0.8 °C isotherm at a depth 6.3 m for a thick dry aeolian sand layer is deeper of 1.3 m than the one for a thick wet aeolian sand layer (Fig. 7d).

As shown in Fig. 7, the formation of an aeolian sand cover on railway embankment slopes is a major factor controlling the permafrost

temperature. It is interesting to note that, even if a thick dry aeolian sand cover increases the ground temperature, the permafrost table is moving upward. A thick dry aeolian sand layer acts as an insulation layer due to its low frozen and unfrozen thermal conductivity. However, even if the permafrost table is deeper for a thick wet aeolian sand cover than for a thick dry aeolian sand cover, a thick wet aeolian sand cover can mitigate and delay the effect of air temperature increase due to climate change on the permafrost warming and thawing, because the permafrost temperatures between 2.0 m and 8.0 m depth are lower in such conditions.

4. Discussions

The heat transfer model used in this study had been verified by comprising with the variation of temperature and Rayleigh number in rock layer, and ground temperature variation in the field experiment in QTP (Yu et al., 2016). The model is sufficient for accurate simulation of the conductive and convective heat transfer in the sand-free and sand-filled rock layer, and the heat propagation in the frozen and thawed soils.

Thermal properties and surface temperature boundary conditions play a significant role in the ground temperatures. Firstly, higher albedo of aeolian sand leads to the greater upward shortwave radiation flux and induces the and induces the colder temperatures than that for other surfaces (Xie et al., 2015; Zhang et al., 2010). Besides, due to its low thermal conductivity, a thick dry aeolian sand layer acting as an insulation layer warm the underlying permafrost. In contrast, higher thermal conductivity of wet aeolian sand benefit the heat transfer between the atmosphere and the ground soils, which lead to more heat extraction in the winter. Thus, a thick wet aeolian sand cover can mitigate and delay the effect of climate change on the permafrost degradation, while dry aeolian sand layer warm the underlying permafrost.

Additionally, the projected change in air temperature in QTP is at the range of 2.2 °C to 2.6 °C $50a^{-1}$ in QTR (Qin et al., 2002), which has been clearly verified by the long-term field observation in QTP, such as a rapid warming tendency of 0.068 °C a^{-1} has been occurring at Wudao Liang in the QTP since 1997 (Chen et al., 2017; Yu et al., 2016). A linear ground surface temperature increasing rate was adopted by majority studies to evaluate the effect of increasing air temperature due to climate change on permafrost warming and thawing (Cheng and Wu, 2007; Lai et al., 2003; Zhang et al., 2015). While, a linear increasing surface temperature ignores the inter-annual variability and does not totally represent the projected climate change. Also, the temperature of embankment subbase and subgrade is a function of air temperature variation, atmospheric radiation, surface moisture content, ground-surface albedo and subsurface soil processes (Glose et al., 2017; Westermann et al., 2009; Yao et al., 2011; Zhang et al., 2013).The aeolian sand layer not only largely change the ground-surface albedo but also alter hydraulic conductivity of top soil layer. Therefore, a surface energy balance model and fully-coupled water flow and heat transfer model should be developed to investigate the performance of CRIE in sandy permafrost regions.

Under a MAAT of −4.5 °C with an increasing rate of 0.052 °C a^{-1}, the aeolian sand clogging and accumulation have an adverse effect on the cooling effect of open CRIE. After the aeolian sand clogging, ground temperatures beneath the open CRIE increase about 1.2 °C and the permafrost table is deeper by 2.5 m (Figs. 4 and 5), compared to the sand-free CRIE. While, for the closed CRIE, the ground temperatures change slightly, at the range of 0.2 °C (Fig. 7). The reason relates to the change of boundary condition and porosity of crushed-rock layer. Without the aeolian sand clogging, the intensive convection of air through the voids of an open CRIE largely increases the effective heat extraction in the embankment subgrade, but air convection in the CRI of closed CRIE is weak. After the aeolian sand clogging and accumulation, the sand-filled crushed rocks prevent wind incursion into the CRI and the zones for air convection largely reduce for the open CRIE. The cooling effect largely depends on the natural convection in the winter. But, for the closed CRIE, the aeolian sand clogging does not occur. After aeolian sand accumulation at the embankment slope and toe, the temperatures change of embankment subgrade are mainly controlled by the surface temperature variation and heat conduction through aeolian sand which mean that the albedo of aeolian sand and thermal conductivity play an important to the permafrost temperature beneath road embankment (Fig. 7).

Furthermore, field investigation showed that aeolian sand can fill into the rock layer of embankment slope and the thickness of sand-filled rock layer can be > 1 m at the toe of embankment. And the obstacle of the embankment change the air flow direction (Chen et al., 2015). On the upwind side, the air flow rises along the embankment slope, while there is an anti-clockwise eddy on the downwind side due to the formation of low-pressure field, which generally induce more accumulation of aeolian sand. Besides, the angle between wind direction and embankment alignment, and duration and speed of wind also impact the accumulation of aeolian sand (Chen et al., 2015; Zhang et al., 2010). Therefore, asymmetry distribution of aeolian sand and dynamic process of aeolian sand deposition should be included in the further studies.

5. Conclusions

Cooling effectiveness of the CRIE is affected by aeolian sand clogging of the voids in the CRI and aeolian sand accumulation on the railway embankment slopes due to wind transport of sand. The performance of this mitigation technique is also affected by the increasing air temperature already occurring in the QTP and anticipated over the next decade. According to the results of numerical modelling of the thermal regime of QTR subbase and subgrade under different conditions presented herein, the following conclusions can be drawn:

(1) The cooling effectiveness of open CRIE can counteract the thermal response of embankment subgrade in a context of climate warming with an increasing rate of 0.052 °C a^{-1}. However, if the voids of the crushed rock interlayer are clogged and covered by aeolian sand, the cooling effectiveness is largely weakened and permafrost warming and thawing can occur underneath the railway embankment.
(2) The decrease in the cooling effectiveness of open the CRIE due to aeolian sand clogging and accumulation has greater impacts on the permafrost table and MAGT underneath the embankment centerline than that at the embankment toe at warmer MAAT. Moreover, the decrease in ice content in a 2-m thick frost-susceptible clay layer located at a depth of 3 m below the natural ground surface induces a deepening of the permafrost table.
(3) The sand accumulation on the railway embankment slopes can change the permafrost conditions underneath the railway embankment. For a 1-m thick dry aeolian sand cover, the permafrost table underneath the railway embankment toes is shallower than any other cases simulated. Moreover, a 1-m thick wet aeolian sand cover induces colder conditions underneath the railway embankment centerline than any other cases simulated.
(4) Results shows that the increase in air temperature due to climate change and aeolian sand deposition weaken cooling effectiveness of CRIE, permafrost will degrade in the coming decades. Melting of ground ice and thaw consolidation can promote thaw-induced embankment subsidence. Therefore, sand-control measures and additional engineering techniques should be adopted to prevent embankment failure in sandy permafrost zone of QTP.

6. Nomenclature

v	velocity m s^{-1}
z	z axis m
T	temperature °C
t	time h
C	heat capacity J m^{-3} K^{-1}
L	latent heat in ice phase transition J m^{-3}
W	water content %
B	temperature increment °C
A	seasonal temperature amplitude °C

6.1. Greek symbols

λ	thermal conductivity W m^{-1} °C^{-1}
ρ	density of the medium kg m^{-3}
φ	phase shift radian
α	rate of climate change °C a^{-1},

6.2. Subscripts

f	frozen state
u	unfrozen state
a	air

Supplementary data to this article can be found online at https://doi.org/10.1016/j.coldregions.2018.07.009.

Acknowledgements

This work was supported by the National Natural Science Foundation of China (41571070), the Fund of the National Key Basic Research and Development Program (2012CB026102), the Funds of Key Research Program of Frontier Sciences of CAS (QYZDY-SSW-DQC011) and fund HHS-TSS-STS-1502. Thanks to China Scholarship Council (CSC) to Lin Chen, PhD scholarship. Meanwhile, thank Prof. Richard Fortier for improving the English of this paper.

References

Carson, J.E., 1963. Analysis of soil and air temperatures by Fourier techniques. J. Geophys. Res. 68 (8), 2217–2232. https://doi.org/10.1029/JZ068i008p02217.

Chen, L., Yu, W.B., Yang, C.S., Yi, X., Liu, W.B., 2014. Conductivity of aeolian sand on the Tibet Plateau based on microstructure. J. Glaciol. Geocryol. 36 (5), 1220–1226. https://doi.org/10.7522/j.issn.1000-0240.2014.0146.

Chen, L., Yu, W., Han, F., Liu, W., Yi, X., 2015. Impacts of aeolian sand on cooling effect of crushed-rock embankment of Qinghai-Tibet Railway. J. Glaciol. Geocryol. 37 (1), 147–155. https://doi.org/10.7522/j.issn.1000-0240.2015.0016. (in Chinese).

Chen, L., Yu, W., Lu, Y., Liu, W., 2017. Numerical simulation on the performance of thermosyphon adopted to mitigate thaw settlement of embankment in Sandy permafrost zone. Appl. Therm. Eng. 128 (5), 1624–1633. https://doi.org/10.1016/j.applthermaleng.2017.09.130.

Cheng, G.D., 2005. A roadbed cooling approach for the construction of Qinghai–Tibet Railway. Cold Reg. Sci. Technol. 42 (2), 169–176. https://doi.org/10.1016/j.coldregions.2005.01.002.

Cheng, G.D., Wu, T.H., 2007. Responses of permafrost to climate change and their environmental significance, Qinghai-Tibet Plateau. J. Geophys. Res. Earth Surf. 112 (F2). https://doi.org/10.1029/2006JF000631.

Darrow, M.M., Jensen, D.D., 2016. Modeling the performance of an air convection embankment (ACE) with thermal berm over ice-rich permafrost, Lost Chicken Creek, Alaska. Cold Reg. Sci. Technol. 130, 43–58. https://doi.org/10.1016/j.coldregions.2016.07.012.

Dong, Y., Pei, W., Liu, G., Jin, L., Chen, D., 2014. In-situ experimental and numerical investigation on the cooling effect of a multi-lane embankment with combined crushed-rock interlayer and ventilated ducts in permafrost regions. Cold Reg. Sci. Technol. 104, 97–105. https://doi.org/10.1016/j.coldregions.2014.05.003.

Doré, G., Niu, F.J., Brooks, H., 2016. Adaptation methods for transportation infrastructure built on degrading permafrost. Permafr. Periglac. Process. 352–364. https://doi.org/10.1002/ppp.1919.

Farouki, O.T., 1981. The thermal properties of soils in cold regions. Cold Reg. Sci. Technol. 5 (1), 67–75. https://doi.org/10.1016/0165-232X(81)90041-0.

Fortier, R., Leblanc, A.-M., Yu, W., 2011. Impacts of permafrost degradation on a road embankment at Umiujaq in Nunavik (Quebec), Canada. Can. Geotech. J. 48 (5), 720–740. https://doi.org/10.1139/t10-101.

Glose, A., Lautz, L.K., Baker, E.A., 2017. Stream heat budget modeling with HFLUX: model development, evaluation, and applications across contrasting sites and seasons. Environ. Model. Softw. 92, 213–228. https://doi.org/10.1016/j.envsoft.2017.02.021.

Goering, D.J., 2003. Passively cooled railway embankments for use in permafrost areas. J. Cold Reg. Eng. 17 (3), 119–133. https://doi.org/10.1061/(ASCE)0887-381X(2003)17:3(119).

Goering, D.J., Kumar, P., 1996. Winter-time convection in open-graded embankments. Cold Reg. Sci. Technol. 24 (1), 57–74. https://doi.org/10.1016/0165-232X(95)00011-Y.

Harden, J.W., Koven, C.D., Ping, C.L., Hugelius, G., David McGuire, A., Camill, P., Jorgenson, T., Kuhry, P., Michaelson, G.J., O'Donnell, J.A., 2012. Field information links permafrost carbon to physical vulnerabilities of thawing. Geophys. Res. Lett. 39 (15). https://doi.org/10.1029/2012GL051958.

Harris, S.A., Pedersen, D.E., 1998. Thermal regimes beneath coarse blocky materials. Permafr. Periglac. Process. 9 (2), 107–120. https://doi.org/10.1002/(SICI)1099-1530(199804/06)9:2<107::AID-PPP277>3.0.CO;2-G.

Hou, Y., Wu, Q., Liu, Y., Zhang, Z., Gao, S., 2015. The thermal effect of strengthening measures in an insulated embankment in a permafrost region. Cold Reg. Sci. Technol. 116, 49–55. https://doi.org/10.1016/j.coldregions.2015.04.003.

Lai, Y., Zhang, L., Zhang, S., Mi, L., 2003. Cooling effect of ripped-stone embankments on Qing-Tibet railway under climatic warming. Chin. Sci. Bull. 48 (6), 598–604. https://doi.org/10.1360/03tb9127.

Lai, Y.M., Zhang, M.Y., Liu, Z.Q., Yu, W.B., 2006. Numerical analysis for cooling effect of open boundary ripped-rock embankment on Qinghai-Tibetan railway. Sci. China Ser. D 49 (7), 764–772. https://doi.org/10.1007/s11430-006-0764-z.

Lai, Y.M., Pei, W.S., Yu, W.B., 2014. Calculation theories and analysis methods of thermodynamic stability of embankment engineering in cold regions. Chin. Sci. Bull. 59 (3), 261–272. https://doi.org/10.1007/s11434-013-0012-9.

Liu, M., Niu, F., Ma, W., Fang, J., Lin, Z., Luo, J., 2017. Experimental investigation on the enhanced cooling performance of a new crushed rock revetment embankment in warm permafrost regions. Appl. Therm. Eng. https://doi.org/10.1016/j.applthermaleng.2017.03.118.

Ma, W., Cheng, G.D., Wu, Q.B., 2009. Construction on permafrost foundations: lessons learned from the Qinghai–Tibet railroad. Cold Reg. Sci. Technol. 59 (1), 3–11. https://doi.org/10.1016/j.coldregions.2009.07.007.

Malenfant-Lepage, J., Doré, G., Fortier, F., 2010. Experimentation of mitigation techniques to reduce the effects of permafrost degradation on transportation infrastructures at Beaver Creek experimental road side (Alaska Highway, Yukon). In: Proceedings 63rd Canadian Geotechnical Conference, Calgary, Alberta, pp. 526–533.

Malenfant-Lepage, J., Doré, G., Fortier, D., Murchison, P., 2012. Thermal performance of the permafrost protection techniques at Beaver Creek experimental road site, Yukon, Canada. In: In Proceedings of the 10th International Conference on Permafrost. Salekhard, Russia, 25–29 June, the Northern Publisher, pp. 261–266.

Mu, Y., Ma, W., Wu, Q., Sun, Z., Liu, Y., 2012. Cooling processes and effects of crushed rock embankment along the Qinghai–Tibet Railway in permafrost regions. Cold Reg. Sci. Technol. 78, 107–114. https://doi.org/10.1016/j.coldregions.2012.01.014.

Qin, D.H., Ding, Y.H., Wang, S.W., 2002. A study of environment change and its impacts in western China. Earth Sci. Front. 9 (2), 321–328.

Sivakumar, M., 2007. Interactions between climate and desertification. Agric. For. Meteorol. 142 (2), 143–155. https://doi.org/10.1016/j.agrformet.2006.03.025.

Solomon, S.S., Qin, D.H., Manning, M., Chen, Z., Marquis, M., Averyt, K.B., Tignor, M., Miller, H.L., 2007. Contribution of Working Group I to the Fourth Assessment Report of the Intergovernmental Panel on Climate Change, 2007. Cambridge University Press, Cambridge.

Sun, B., Yang, L., Liu, Q., Wang, W., Xu, X., 2011. Experimental study on cooling enhancement of crushed rock layer with perforated ventilation pipe under air-tight top surface. Cold Reg. Sci. Technol. 68 (3), 150–161. https://doi.org/10.1016/j.coldregions.2011.06.009.

Tao, W.-Q., 2001. Numerical Heat Transfer. Xi'an Jiaotong University Press, Xi'an.

Westermann, S., Lüers, J., Langer, M., Piel, K., Boike, J., 2009. The annual surface energy budget of a high-arctic permafrost site on Svalbard, Norway. Cryosphere 3 (2), 245. https://doi.org/10.5194/tc-3-245-2009.

Wu, Q., Liu, Y., Zhang, J., Tong, C., 2002. A review of recent frozen soil engineering in permafrost regions along Qinghai-Tibet Highway, China. Permafr. Periglac. Process. 13 (3), 199–205. https://doi.org/10.1002/ppp.420.

Wu, Q.B., Lu, Z.J., Zhang, T.J., Ma, W., Liu, Y.Z., 2008. Analysis of cooling effect of crushed rock-based embankment of the Qinghai-Xizang Railway. Cold Reg. Sci. Technol. 53 (3), 271–282. https://doi.org/10.1016/j.coldregions.2007.10.004.

Wu, Q., Yu, W., Jin, H., 2017. No protection of permafrost due to desertification on the Qinghai–Tibet Plateau. Sci. Rep. 7. https://doi.org/10.1038/s41598-017-01787-0.

Xie, S., Qu, J., Lai, Y., Xu, X., Pang, Y., 2015. Key evidence of the role of desertification in protecting the underlying permafrost in the Qinghai–Tibet Plateau. Sci. Rep. 5. https://doi.org/10.1038/srep15152.

Xie, S., Qu, J., Pang, Y., 2017. Dynamic wind differences in the formation of sand hazards at high-and low-altitude railway sections. J. Wind Eng. Ind. Aerodyn. 169, 39–46.

https://doi.org/10.1016/j.jweia.2017.07.003.
Xu, J., Goering, D.J., 2008. Experimental validation of passive permafrost cooling systems. Cold Reg. Sci. Technol. 53 (3), 283–297. https://doi.org/10.1016/j.coldregions.2007.09.002.
Xu, X.Z., Wang, J.C., Zhang, L.X., 2001. Physics of Frozen Soils. Science Press, Beijing.
Yao, J., Zhao, L., Gu, L., Qiao, Y., Jiao, K., 2011. The surface energy budget in the permafrost region of the Tibetan Plateau. Atmos. Res. 102 (4), 394–407. https://doi.org/10.1016/j.atmosres.2011.09.001.
Yu, W.B., Lai, Y.M., Zhang, X.F., Zhang, S.J., Xiao, J.Z., 2004. Laboratory investigation on cooling effect of coarse rock layer and fine rock layer in permafrost regions. Cold Reg. Sci. Technol. 38 (1), 31–42. https://doi.org/10.1016/S0165-232X(03)00061-2.
Yu, W.B., Liu, W.B., Lai, Y.M., Chen, L., Yi, X., 2014. Nonlinear analysis of coupled temperature-seepage problem of warm oil pipe in permafrost regions of Northeast China. Appl. Therm. Eng. 70 (1), 988–995. https://doi.org/10.1016/j.applthermaleng.2014.06.028.
Yu, W.B., Liu, W.B., Chen, L., Yi, X., Han, F.L., Hu, D., 2016. Evaluation of cooling effects of crushed rock under sand-filling and climate warming scenarios on the Tibet Plateau. Appl. Therm. Eng. 92, 130–136. https://doi.org/10.1016/j.applthermaleng.2015.09.030.
Zhang, M.Y., 2007. Study on Long-Term Thermal Stability of Air-Cooled Subgrade in Permafrost Regions. PhD thesis Thesis. University of Chinese Academy of Sciences, Lanzhou.
Zhang, M., Lai, Y., Gao, Z., Yu, W., 2006a. Influence of boundary conditions on the cooling effect of crushed-rock embankment in permafrost regions of Qinghai–Tibetan Plateau. Cold Reg. Sci. Technol. 44 (3), 225–239. https://doi.org/10.1016/j.coldregions.2005.12.002.
Zhang, M.Y., Lai, Y.M., Niu, F.J., He, S.S., 2006b. A numerical model of the coupled heat transfer for duct-ventilated embankment under wind action in cold regions and its application. Cold Reg. Sci. Technol. 45 (2), 103–113. https://doi.org/10.1016/j.coldregions.2006.03.002.
Zhang, K.C., Qu, J.J., Liao, K.T., Niu, Q.H., Han, Q.J., 2010. Damage by wind-blown sand and its control along Qinghai-Tibet Railway in China. Aeolian Res. 1 (3), 143–146. https://doi.org/10.1016/j.aeolia.2009.10.001.
Zhang, Y., Cheng, G., Li, X., Han, X., Wang, L., Li, H., Chang, X., Flerchinger, G., 2013. Coupling of a simultaneous heat and water model with a distributed hydrological model and evaluation of the combined model in a cold region watershed. Hydrol. Process. 27 (25), 3762–3776. https://doi.org/10.1002/hyp.9514.
Zhang, M.Y., Zhang, X.Y., Li, S.Y., Wu, D.Y., Pei, W.S., Lai, Y.M., 2015. Evaluating the cooling performance of crushed-rock interlayer embankments with unperforated and perforated ventilation ducts in permafrost regions. Energy 93, 874–881. https://doi.org/10.1016/j.energy.2015.08.059.
Zhang, M., Lai, Y., Wu, Q., Yu, Q., Zhao, T., Pei, W., Zhang, J., 2016. A full-scale field experiment to evaluate the cooling performance of a novel composite embankment in permafrost regions. Int. J. Heat Mass Transf. 95, 1047–1056. https://doi.org/10.1016/j.ijheatmasstransfer.2015.12.067.
Zhao, M., Miao, M.Q., Wang, Y.C., 1991. Boundary Layer Meteorology. China Meteorological Press, Beijing.
Zhu, L.N., 1988. Study of the adherent layer on different types of ground in permafrost regions on the Qinghai-Xizang Plateau. J. Glaciol. Geocryol. 1, 35–39 (in Chinese).